Spin-valley-resolved energy spectra of quantum dots in the graphene/transition metal dichalcogenides system

Qiang Cheng [1,2] and Qing-Feng Sun [2,3,4,*]

[1] *School of Science, Qingdao University of Technology, Qingdao, Shandong 266520, China*

[2] *International Center for Quantum Materials, School of Physics, Peking University, Beijing 100871, China*

[3] *Collaborative Innovation Center of Quantum Matter, Beijing 100871, China*

[4] *CAS Center for Excellence in Topological Quantum Computation, University of Chinese Academy of Sciences, Beijing 100190, China*

(Received 24 December 2021; revised 12 April 2022; accepted 13 April 2022; published 22 April 2022)

We study the energy spectra of Dirac fermions confined in the quantum dot formed in the graphene/transition metal dichalcogenides (TMD) system under a perpendicular magnetic field. The obtained spin-valley polarized spectra can be classified into three types according to the values of the energy gap, which strongly depends on the pseudospin potential and the valley-dependent spin-orbit coupling peculiar to the electronic structure of the graphene/TMD system. For the first case, the electrons for both valleys and both spins possess linear dispersion. The energy spectra of the quantum dot exhibit sudden jumps of levels due to the Berry phase jumps. For the second case, the electrons for the $K(K')$ valley with up (down) spin have linear dispersion while the electrons for the $K(K')$ valley with down (up) spin have parabolic dispersion. The sudden jumps and the degeneracy-splitting-recombination behaviors of levels coexist in the energy spectra. The latter behavior is a result of the continuous change of the Berry phase. For the third case, the electrons for both valleys and both spins have parabolic dispersion. The degeneracy-splitting-recombination behaviors make the energy spectra both spin and valley distinguished. In addition, the evolutions of the levels from the sudden jumps to the continuous changes by adjusting the valley-dependent spin-orbit coupling and the pseudospin potential are also investigated. These results provide the possibility to control the specific spin-valley freedom of electrons in the graphene/TMD system using the quantum dot setup.

DOI: 10.1103/PhysRevB.105.165427

I. INTRODUCTION

A graphene quantum dot under a perpendicular magnetic field has attracted much research interest both for the monolayer and bilayer to reveal the behaviors of the confined Dirac fermions [1–5]. For the graphene monolayer, the projection of the Berry curvature in the momentum space is point shaped [6]. The Berry phase jump from 0 to π can be realized through changing the value of the magnetic field. For the graphene bilayer, the projection of the Berry curvature is ring shaped [6]. The Berry phase can be continuously tuned from 0 to 2π. Theoretical studies showed that the controllable Berry phase can lead to peculiar spectroscopic features, which are the sudden separation of the angular-momentum sublevels for the monolayer [7] and the degeneracy-splitting-crossing-splitting-degeneracy process of valley levels for the bilayer [8]. Soon after, these features were demonstrated experimentally by the scanning tunneling spectroscopy measurement [9,10], which paved the way for the design of devices based on the valley degree of freedom in valleytronics. However, the spin degree of freedom in monolayer and bilayer graphene quantum dots is still degenerate. How to obtain the spin-valley-resolved energy spectra in the two-dimensional hexagonal lattice system is a question to be addressed in condensed matter physics, which will establish the foundation of spin-valley-based electronics.

Similar to graphene, the TMD monolayer is another class of two-dimensional material with two well-separated inequivalent valleys located at the K point and K' point of the Brillouin zone. Beyond graphene, the TMD monolayer possesses a strong pseudospin potential and spin-orbit coupling, which can lead to the coupling of the spin and valley degrees of freedom absent in graphene [11–13]. In each valley, the electrons are spin polarized while the electrons from both valleys satisfy the time-reversal symmetry. The coupling of spin and valley in the TMD monolayer can bring a lot of unique physics in the Hall effect [14–16], magnetic response [17,18], and transport properties [19]. The relevance of the tunable Berry curvature to the valley/spin Hall effect and the Nernst effect is also uncovered [20–22].

However, the pseudospin potential and the spin-orbit coupling in the TMD monolayer have the order of magnitude of hundreds of meV, which hinders the research on the low-energy physics of the TMD monolayer. Fortunately, the tunable pseudospin potential and the spin-orbit coupling can be realized in the proximity system formed by the graphene on TMDs [23–26]. The proximity system can be described by the Hamiltonian of the TMD monolayer but has the pseudospin potential and the spin-orbit coupling of the meV order. The graphene/TMD system with the tunable potential and spin-orbit coupling make it possible to

*sunqf@pku.edu.cn

investigate the spin-valley-based low-energy physics in two-dimensional materials [27,28]. Recently, it has been found that similar electronic properties can also be realized in a graphene/hexagonal BN (or AlN, GaN, h-VN) system [29,30] or the TMD/graphene/$h-$BN system [31].

In this paper, we study the regulation of the Berry phase and the energy spectra of the quantum dot in the graphene/TMD system under a perpendicular field, which is still blank in condensed matter physics. We focus on three sets of typical parameter values for the pseudospin potential and valley-dependent spin-orbit coupling to tune the Berry curvature. For the first situation, the dispersion of electrons shows the form of the gapless Dirac cone both for two valleys and two spins. The Berry curvature in the momentum space is point shaped, which is the same as that for the monolayer graphene. The sudden jumps and separations of levels emerge in the energy spectra due to the Berry phase jumps from 0 to π or π to 0 as the field is increased.

For the second situation, the electrons from valley K with up spin or from valley K' with down spin still have the sudden jumps of levels in their energy spectra due to the Dirac cone dispersions and the Berry phase jumps. However, the energy bands for the electrons from valley K with down spin or from valley K' with up spin are of parabolic dispersion, which are similar to those for monolayer graphene with the staggered potential. The levels exhibit degeneracy-splitting-recombination behaviors. As a result, the sudden jumps and the degeneracy-splitting-recombination behaviors can be simultaneously realized in the graphene/TMD system. The coexistence of the two distinct behaviors of the levels still cannot be obtained in the graphene monolayer or bilayer.

For the third situation, the energy bands have parabolic dispersion both for the two spins and the two valleys. The energy spectra with the degeneracy-splitting-recombination behaviors can be obtained for each spin-valley index and are polarized both for spin and valley. The valley-polarized energy spectra for $K\uparrow$ and $K'\downarrow$ electrons are symmetric about the magnetic filed $B=0$. The spin-polarized energy spectra for $K\uparrow$ and $K\downarrow$ electrons have a relative translation. These spin-valley-resolved energy spectra may help realize the manipulation of the electrons with the specific valley and spin, which cannot be realized in the graphene monolayer or bilayer with the spin degeneracy. Besides the energy spectra for the above three situations, we also discuss the realization of the switches between the sudden jumps and continuous changes of the levels by tuning the valley-dependent spin-orbit coupling and the pseudospin potential.

The organization of this paper is as follows. In Sec. II, we give the model of the graphene/TMD system and show in detail the derivations of the Berry curvatures, the Berry phase, and the expression of LDOS. In Sec. III, we present the numerical results for the energy bands, the Berry phase, and LDOS for the quantum dot. The features of the energy spectra are discussed and explained physically. Section IV concludes this paper.

II. MODEL AND FORMULATION

We consider the graphene/TMD system schematically shown in Fig. 1. The system is comprised of monolayer graphene and the TMD substrate. The pseudospin potential and the valley-dependent spin-orbit coupling can be proximity induced in graphene from the TMD substrate. The tight-binding Hamiltonian for the system can be written as [27,28]

$$\mathcal{H}=-t\sum_{\langle i,j\rangle\rho}c_{i\rho}^{+}c_{j\rho}+\sum_{i\rho}\Delta\xi_{\beta}c_{i\rho}^{+}c_{i\rho}+\frac{i}{3\sqrt{3}}\sum_{\langle\langle i,j\rangle\rangle\rho\mu}\lambda_{\beta}v_{ij}c_{i\rho}^{+}\sigma_{\rho\mu}^{z}c_{j\mu}. \quad (1)$$

Here, $c_{i\rho}^{+}(c_{i\rho})$ is the creation (annihilation) operator for an electron on lattice site i with spin ρ. The first term denotes the nearest-neighbor hopping with its amplitude $-t$. The second term represents the on-site staggered potential with $\xi_A=1$ for sublattice A and $\xi_B=-1$ for sublattice B. The third term is the sublattice-dependent spin-orbit coupling with coupling magnitudes λ_A and λ_B. One has $v_{ij}=1$ for the counterclockwise hopping and $v_{ij}=-1$ for the clockwise hopping between the next-nearest-neighbor sites. The symbol σ^z denotes the z component of the Pauli matrix $\boldsymbol{\sigma}$.

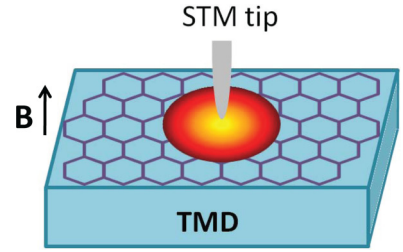

FIG. 1. The schematic diagram of the graphene/TMD system formed by graphene (the hexagonal lattice) on the TMD substrate. The quantum dot (the circular bright area) can be created by a STM tip on the system. A perpendicular field is applied to tune the Berry phase of the fermions confined in the quantum dot.

The quantum dot in the graphene/TMD system can be created by a scanning tunneling microscope (STM) tip [9,10,32] as shown in Fig. 1. We will introduce the parabolic potential $U(r)=\kappa r^2$ to model the circular quantum dot with its center at $r=0$. It is just an extra on-site potential in the tight-binding Hamiltonian. The perpendicular field $\boldsymbol{B}$ is imposed to control the Berry phase of the fermions confined in the quantum dot. We will introduce its vector $\boldsymbol{A}$ satisfying the relation $\mathbf{B}=\nabla\times\boldsymbol{A}$. The effect of the field can be included in the nearest-neighbor hopping as a phase $\phi_{ij}=\frac{e}{\hbar}\int_i^j\boldsymbol{A}\cdot d\boldsymbol{l}$. Next, we will use the low-energy effective Hamiltonian derived from Eq. (1) to study the physics of the electrons confined in the dot. The direct calculations can also be carried out from the tight-binding Hamiltonian for the nanoribbon of the graphene/TMD system. The obtained results will show some derivations from those for the low-energy effective Hamiltonian. The derivations mainly originate from the finite size of the nanoribbon and the high-energy levels considered [8]. However, the fundamental characteristics of the energy spectra in this paper such as their spin-valley polarization will not be changed.

A. Berry curvature

The low-energy effective Hamiltonian describing the graphene/TMD system with the pseudospin potential and the valley-dependent spin-orbit coupling can be written in the pseudospin space (denoted by sublattices 1 and 2) as

$$H_0^{\xi s_z} = \begin{pmatrix} \Delta + \xi s_z \lambda_1 & \hbar v_F(\xi k_x - i k_y) \\ \hbar v_F(\xi k_x + i k_y) & -\Delta + \xi s_z \lambda_2 \end{pmatrix}, \tag{2}$$

with $\xi = \pm 1$ for the K and K' valleys and $s_z = \pm 1$ for the spin up and spin down. The Fermi velocity $v_F = -\frac{3at}{2\hbar}$ with a the lattice constant is taken as 5×10^5 m/s for the graphene/TMD system [14,20,24,33]. Larger values of the Fermi velocity such as that in Refs. [24,29] will not fundamentally change our physical results. The pseudospin potential Δ is independent on the spin and valley indices. The valley dependent spin-orbit couplings are denoted by $\lambda_1 = \lambda_A$ and $\lambda_2 = -\lambda_B$ for the two pseudospins (sublattices). As the treatment in Ref. [34], we take generic values of Δ, λ_1 and λ_2 to explore the peculiar spin-valley energy spectra in the quantum dot.

The eigenvalues of the Hamiltonian in Eq. (2) are given by

$$E_{\xi s_z \pm} = \pm\sqrt{\hbar^2 v_F^2 k^2 + \Delta_{\xi s_z}^2} + \xi s_z \frac{\lambda_1 + \lambda_2}{2}, \tag{3}$$

where $\pm$ denote the conduction and valence bands, $k^2 = k_x^2 + k_y^2$, and $\Delta_{\xi s_z} = \Delta + \xi s_z \frac{\lambda_1 - \lambda_2}{2}$ is the gap for the electrons with the indices ξ and s_z. For each valley, the energy bands are spin split. However, the time-reversal symmetry is still obeyed. The corresponding normalized eigenvectors can be written as

$$\psi_{\xi s_z \pm} = \begin{pmatrix} \pm\sqrt{\frac{\sqrt{\hbar^2 v_F^2 k^2 + \Delta_{\xi s_z}^2} \pm \Delta_{\xi s_z}}{2\sqrt{\hbar^2 v_F^2 k^2 + \Delta_{\xi s_z}^2}}}\, \frac{\xi k_x - i k_y}{k} \\ \sqrt{\frac{\sqrt{\hbar^2 v_F^2 k^2 + \Delta_{\xi s_z}^2} \mp \Delta_{\xi s_z}}{2\sqrt{\hbar^2 v_F^2 k^2 + \Delta_{\xi s_z}^2}}} \end{pmatrix}. \tag{4}$$

The Berry curvatures, which are defined as $F_{\xi s_z \pm}(k_x, k_y) = \frac{\partial a_y(k_x,k_y)}{\partial k_x} - \frac{\partial a_x(k_x,k_y)}{\partial k_y}$ with $a_x(k_x, k_y) = i\langle\psi_{\xi s_z \pm}|\frac{\partial}{\partial k_x}|\psi_{\xi s_z \pm}\rangle$ and $a_y(k_x, k_y) = i\langle\psi_{\xi s_z \pm}|\frac{\partial}{\partial k_y}|\psi_{\xi s_z \pm}\rangle$, can be calculated as

$$F_{\xi s_z \pm}(k_x, k_y) = \mp\xi \frac{\hbar^2 v_F^2 \Delta_{\xi s_z}}{2\left(\hbar^2 v_F^2 k^2 + \Delta_{\xi s_z}^2\right)^{3/2}}. \tag{5}$$

We have $F_{\xi s_z \pm}(k_x, k_y) + F_{\bar{\xi}\bar{s}_z \pm}(k_x, k_y) = 0$ with $\bar{\xi} = -\xi$ and $\bar{s}_z = -s_z$ due to the time-reversal symmetry.

B. Berry phase

Now, we introduce the parabolic potential $U(r) = \kappa r^2$ to model the circular quantum dot. The magnetic field $\mathbf{B}$ perpendicular to the system as shown in Fig. 1 is applied. Its vector potential is chosen as $\mathbf{A} = (A_x, A_y, A_z) = B(-y, x, 0)/2$ with $\mathbf{B} = \nabla \times \mathbf{A} = (0, 0, B)$. The Hamiltonian under the parabolic potential and vector potential can be written as

$$H^{\xi s_z} = \begin{pmatrix} \Delta + \xi s_z \lambda_1 + U(r) & v_F(\xi \Pi_x - i\Pi_y) \\ v_F(\xi \Pi_x + i\Pi_y) & -\Delta + \xi s_z \lambda_2 + U(r) \end{pmatrix}, \tag{6}$$

with the kinetic momentum operators $\mathbf{\Pi} = (\Pi_x, \Pi_y) = (-i\hbar\partial_x - A_x, -i\hbar\partial_y - A_y)$. We replace the operators $(-i\hbar\partial_x, -i\hbar\partial_y)$ by the symbols (p_x, p_y) according to the Weyl correspondence [35]. The Hamiltonian in Eq. (6) will become its classical edition. The electronic bands can be solved as

$$E_{\xi s_z} = \sqrt{v_F^2 \Pi^2 + \Delta_{\xi s_z}^2} + \frac{\xi s_z(\lambda_1 + \lambda_2)}{2} + \kappa r^2 \tag{7}$$

through diagonalizing the classical Hamiltonian.

In the polar coordinate system, we express the kinetic momentum as

$$\Pi_r = p_r, \quad \Pi_\theta = \frac{p_\theta}{r} - \frac{eBr}{2}, \tag{8}$$

where the symbol p_θ denotes the conserved angular momentum with its eigenvalues $M\hbar$ (see Sec. II C). Substituting $\Pi^2 = \Pi_r^2 + \Pi_\theta^2$ into Eq. (7), we can obtain the motion equation in the radial direction:

$$\Pi_r^2 = \frac{\left(E - \kappa r^2 - \xi s_z \frac{\lambda_1 + \lambda_2}{2}\right)^2 - \Delta_{\xi s_z}^2}{v_F^2} - \left(\frac{M\hbar}{r} - \frac{eBr}{2}\right)^2. \tag{9}$$

The motion characterized by the equation is confined between the inner and outer turning radii, denoted by r_1 and r_2, in the radial direction. The turning radii can be solved from the condition $\Pi_r = 0$. They determine a closed path in the momentum space spanned by (Π_x, Π_y) through the coordinates (Π_r, Π_θ) as functions of $r \in [r_1, r_2]$.

We discretize the closed path into N sites. The corresponding eigenstate $|\Pi_{xj}, \Pi_{yj}\rangle$ for the jth site can be obtained by solving the equation

$$H^{\xi s_z}|\Pi_{xj}, \Pi_{yj}\rangle = E_j|\Pi_{xj}, \Pi_{yj}\rangle. \tag{10}$$

Here, the Hamiltonian $H^{\xi s_z}$ is the one in Eq. (6) in the absence of $U(r)$. The Berry phase can be calculated with the following expression [36]:

$$\gamma = i\sum_{j=1}^{N-1} \log\langle\Pi_{xj}, \Pi_{yj}|\Pi_{xj+1}, \Pi_{yj+1}\rangle. \tag{11}$$

Here, $|\Pi_{xj}, \Pi_{yj}\rangle$ is the eigenstate on an equienergy contour with a wave vector around the Dirac point. The Berry phase describes the acquired phase when the wave vector is evolved.

C. Local density of states

In the polar coordinate system, the Hamiltonian in Eq. (6) can be changed into

$$H^{\xi s_z} = \begin{pmatrix} \Delta + \xi s_z \lambda_1 + U(r) & L_1 \\ L_2 & -\Delta + \xi s_z \lambda_2 + U(r) \end{pmatrix}, \tag{12}$$

where $L_1 = v_F e^{-\xi i\theta}(-\xi i\hbar\frac{\partial}{\partial r} - \frac{\hbar}{r}\frac{\partial}{\partial\theta} + i\frac{eBr}{2})$ and $L_2 = v_F e^{\xi i\theta}(-\xi i\hbar\frac{\partial}{\partial r} + \frac{\hbar}{r}\frac{\partial}{\partial\theta} - i\frac{eBr}{2})$ with the polar radius r and the polar angle θ. We define the angular momentum operator as

$$J_z^{\xi s_z} = L_z + \xi\frac{\hbar}{2}\tau_z + s_z\frac{\hbar}{2}\tau_0, \tag{13}$$

where the orbital angular momentum $L_z = -i\hbar\frac{\partial}{\partial_\theta}$ and τ_0 and τ_z are the Pauli matrices in the pseudospin space. It is easy to prove that the angular momentum operator is commutative

with the Hamiltonian $H^{\xi s_z}$. Their common wave function can be expressed as

$$\Psi_M^{\xi s_z} = \frac{e^{iM\theta}}{\sqrt{r}} \begin{pmatrix} a_{\xi s_z}(r) e^{-i(\xi + s_z)\theta/2} \\ i b_{\xi s_z}(r) e^{i(\xi - s_z)\theta/2} \end{pmatrix}, \tag{14}$$

where the integer number M is the angular momentum quantum number.

Substituting the wave function into the eigenequation $H^{\xi s_z}\Psi_M^{\xi s_z}(r) = E\Psi_M^{\xi s_z}$, we can obtain the equation $\tilde{H}^{\xi s_z}\Phi^{\xi s_z}(r) = E\Phi^{\xi s_z}(r)$ satisfied by the radial eigenstate $\Phi^{\xi s_z}(r) = (a_{\xi s_z}(r), b_{\xi s_z}(r))^T$. The radial Hamiltonian is given by

$$\tilde{H}^{\xi s_z} = \begin{pmatrix} \Delta + \xi s_z \lambda_1 + U(r) & \tilde{L}_1 \\ \tilde{L}_2 & -\Delta + \xi s_z \lambda_2 + U(r) \end{pmatrix}, \tag{15}$$

with $\tilde{L}_1 = \xi v_F \hbar \frac{\partial}{\partial_r} + \frac{(M - \frac{s_z}{2})\hbar}{r} - \frac{eBr}{2}$ and $\tilde{L}_2 = -\xi v_F \hbar \frac{\partial}{\partial_r} + \frac{(M - \frac{s_z}{2})\hbar}{r} - \frac{eBr}{2}$. For a given quantum number M, the contribution to the LDOS at r from the valley ξ and the spin s_z can be expressed as

$$D_M^{\xi s_z}(B, E) = \sum_\alpha \left\langle \left| \Phi_\alpha^{\xi s_z}(r) \right|^2 \right\rangle_{\lambda_d} \delta_\eta(E - E_\alpha), \tag{16}$$

with $\delta_\eta(E) = \eta/[\pi(E^2 + \eta^2)]$ and $\langle |\Phi_\alpha^{\xi s_z}(r)|^2 \rangle_{\lambda_d} = \sqrt{\frac{2}{\pi}} \frac{1}{\lambda_d} \int_0^\infty dr' |\Phi_\alpha^{\xi s_z}(r')|^2 e^{-(r'-r)^2/2\lambda_d^2}$. Here α indicates the radial eigenstates. The symbols λ_d and η denote the finite broadenings of the position r and energy E, respectively. The total LDOS is given by

$$D(B, E) = \sum_{\xi s_z} D^{\xi s_z}(B, E), \tag{17}$$

where $D^{\xi s_z}(B, E) = \sum_M D_M^{\xi, s_z}(B, E)$ is the LDOS for the valley ξ and the spin s_z contributed from all values of M. In our calculations, we will take $\kappa = 30\,\text{eV}/\mu\text{m}^2$, $\eta = 4.4$ meV, and $\lambda_d = 2.2$ nm. The calculation range in the radial direction is chosen as $0 \leqslant r \leqslant 333$ nm. Equation (15) is solved using the finite difference method and the calculation range will be divided into 667 points. To highlight the levels, we will calculate the second partial derivative of the LDOS with respect to E instead of the LDOS itself.

III. RESULTS AND DISCUSSIONS

If we chose $\Delta = 0$ and $\lambda_{1,2} = 0$, the Hamiltonian in Eq. (2) degenerates into the one for the monolayer graphene with both spin and valley degeneracies. If we chose $\Delta \neq 0$ and $\lambda_{1,2} = 0$, the Hamiltonian for the monolayer graphene with the staggered potential Δ will be obtained. The spin and valley degeneracies still hold. The quantum dot of the graphene/TMD system here will be very different due to the presence of the nonzero valley dependent spin-orbit couplings $\lambda_{1,2}$.

Before presenting the numerical results, we first give some basic properties of the LDOS in the quantum dot of the graphene/TMD system. From the expression of the angular momentum in Eq. (13), it is found that the main contributions to the LDOS $D^{K\uparrow}(B, E)$ at the central position with $r = 0$ of the circular quantum dot originate from the $M = 1$ state for sublattice 1 and the $M = 0$ state for sublattice 2 while the main contributions to $D^{K\downarrow}(B, E)$ originate from the $M = 0$ state for sublattice 1 and the $M = -1$ state for sublattice 2. Due to the time-reversal relation between the two valleys, we also have $T\Psi_M^{\xi s_z}(B, E) = \Psi_{-M}^{\bar{\xi}\bar{s}_z}(-B, E)$. As a result, the M-dependent LDOS $D_M^{\xi s_z}(B, E)$ and $D_{-M}^{\bar{\xi}\bar{s}_z}(B, E)$ are symmetric about $B = 0$. Next, we present the numerical results for three situations and then discuss the evolutions of the energy spectra with the pseudospin potential and spin-orbit coupling.

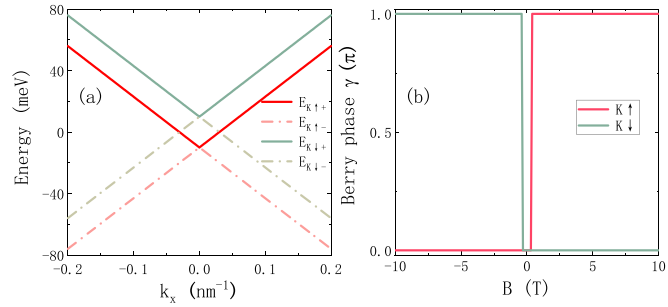

FIG. 2. (a) The energy bands of the graphene/TMD system for valley K under the parameters $\Delta = 0$, $\lambda_1 = -10$ meV and $\lambda_2 = -10$ meV. Both spin-up and spin-down electrons have linear dispersion. (b) The Berry phase jumps from 0 to π for spin-up electrons and from π to 0 for spin-down electrons when the field is increased from $-10T$ to $10T$. The quantum number M is taken as 1 for $K\uparrow$ and -1 for $K\downarrow$. The energy of electrons is taken as $E = 120$ meV.

A. $\Delta_{\xi s_z} = 0$ and $\Delta = 0$

If the conditions of the gap $\Delta_{\xi s_z} = 0$ and the pseudospin potential $\Delta = 0$ are simultaneously satisfied, we will have $\lambda_1 = \lambda_2$. For definiteness, we take $\lambda_1 = -10$ meV and $\lambda_2 = -10$ meV here. The Hamiltonian in Eq. (2) becomes gapless, similar to the graphene monolayer. In this situation, the dispersions for the electrons in the graphene/TMD system consist of two spin-split Dirac cones at each valley as shown in Fig. 2(a). From Eq. (5), one can find that the Berry curvatures for both valleys become zero in the momentum space except for $k = 0$, i.e., the K and K' points in the Brillouin zone. The point-shaped Berry curvatures will cause the Berry phase jump as shown in Fig. 2(b). As we have discussed, the inner and outer turning radii r_1 and r_2 will form the closed path in the momentum space. For the $K\uparrow$ electrons with $M = 1$, if the field is smaller than a critical value, the closed path will not enclose the point $k = 0$. On the other hand, the $k = 0$ point will be enclosed by the closed path when the field is larger than the critical value. The Berry phase γ, as the flux of the Berry curvature, will experience the jump from 0 to π as the magnetic field is changed across the positive critical value. For the $K\downarrow$ electrons with $M = -1$, the Berry phase γ will experience the jump from π to 0 as the field is changed across the negative critical value, as shown in Fig. 2(b). According to the Einstein-Brillouin-Keller quantum rule [7–10,32],

$$\frac{1}{\hbar} \oint_{C_r} \Pi_r dr = 2\pi(n + \delta) - \gamma, \tag{18}$$

the jump of the Berry phase γ will lead to the sudden jump of the energy level. Here, n is an integer number, δ is the Maslov

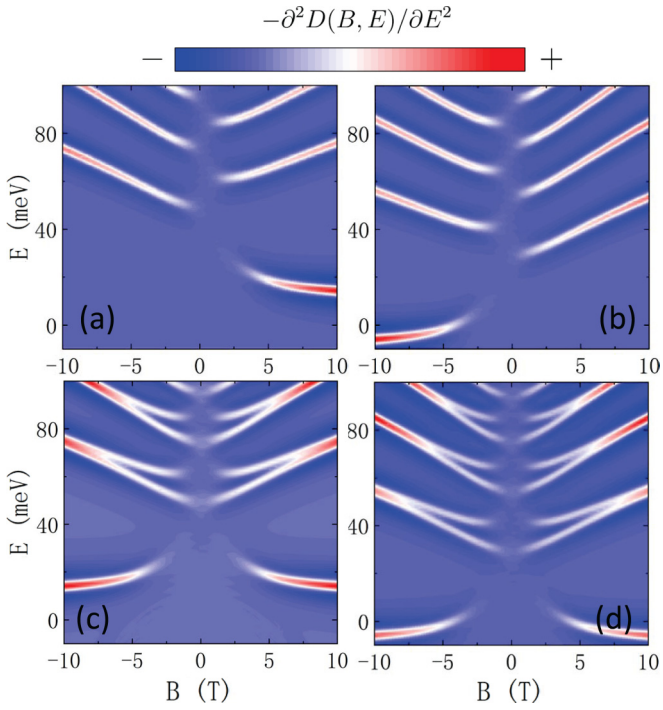

FIG. 3. The LDOS for (a) the valley K and spin $\uparrow$ electrons with $M = 1$ and (b) the valley K and spin $\downarrow$ electrons with $M = -1$. (c) The LDOS $D^{K\uparrow}(B,E) + D^{K'\downarrow}(B,E)$ and (d) the LDOS $D^{K\downarrow}(B,E) + D^{K'\uparrow}(B,E)$ contributed from $-10 \leqslant M \leqslant 10$. The other parameters are taken as $\Delta = 0$, $\lambda_1 = -10$ meV and $\lambda_2 = -10$ meV. The LDOSs at the central position with $r = 0$ of the circular quantum dot are shown here.

index and C_r is the trajectory loop mapped from the confined motion in the radial direction to a torus [8,9]. Figure 3 shows the LDOS at the central position of the quantum dot with $r = 0$. There are two characteristics of the energy spectra in Figs. 3(a) and 3(b). First, the critical field for the $K\uparrow$ electrons with $M = 1$ is positive while it is negative for the $K\downarrow$ electrons with $M = -1$. Second, the jumps of the levels in Fig. 3(a) are the sudden decreases when the field is increased from $-10T$ to $10T$. However, the sudden rises happens in Fig. 3(b). The two characteristics are consistent with the Berry phase jumps in Fig. 2(b).

Due to the time-reversal relation between the two valleys, the LDOS for the $K'\uparrow$ ($K'\downarrow$) electrons and that for the $K\downarrow$ ($K\uparrow$) electrons are symmetric about $B = 0$, i.e., $D^{K\uparrow}(B,E) = D^{K'\downarrow}(-B,E)$ and $D^{K\downarrow}(B,E) = D^{K'\uparrow}(-B,E)$. If we consider the contributions from different values of the quantum number $M(-10 \leqslant M \leqslant 10)$, the LDOS $D^{K\uparrow}(B,E) + D^{K'\downarrow}(B,E)$ and $D^{K\downarrow}(B,E) + D^{K'\uparrow}(B,E)$ with the sudden level separations will be obtained as given in Figs. 3(c) and 3(d), respectively. From Figs. 3(c) and 3(d), we can find the energy spectra are spin-valley polarized. The LDOS $D^{K\uparrow}(B,E) + D^{K'\downarrow}(B,E)$ is moved up while $D^{K\downarrow}(B,E) + D^{K'\uparrow}(B,E)$ is moved down. Actually, one can well distinguish the energy spectra in Fig. 3(c) and those in Fig. 3(d) by tuning the valley-dependent spin-orbit couplings λ_1 and λ_2 under the conditions $\Delta_{\xi s_z} = 0$ and $\Delta = 0$.

However, one cannot distinguish $D^{K\uparrow}(B,E)$ and $D^{K'\downarrow}(B,E)$ or $D^{K\downarrow}(B,E)$ and $D^{K'\uparrow}(B,E)$ because they are

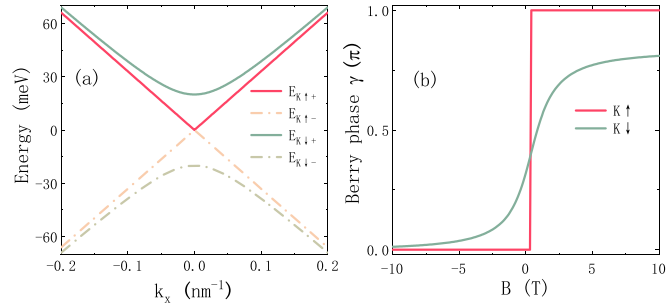

FIG. 4. (a) The energy bands for the valley K under the parameters $\Delta = 10$ meV, $\lambda_1 = -10$ meV and $\lambda_2 = 10$ meV. The electrons with spin $\uparrow$ have linear dispersion while those with spin $\downarrow$ have parabolic dispersion. (b) The jump of Berry phase from 0 to π for the electrons with spin $\uparrow$ and the continuous change of Berry phase from 0 to π for the electrons with spin $\downarrow$. Other parameters are taken as $M = 1$ and $E = 120$ meV.

degenerate if $\Delta = 0$ and $\lambda_1 = \lambda_2$. We analyze the physical origin taking $D^{K\uparrow}(B,E)$ as an example. The unitary matrix $(-\tau_y)$ with τ_y the Pauli matrix in the pseudospin space can change the radial Hamiltonian $\tilde{H}_M^{K\uparrow}(B)$ into $\tilde{H}_{-M+1}^{K\uparrow}(-B)$ in Eq. (15). The LDOS $D^{K\uparrow}(B,E)$ itself as the sum of the contributions from different M is symmetric about $B = 0$, which will lead to $D^{K\uparrow}(B,E) = D^{K'\downarrow}(B,E) = D^{K\uparrow}(-B,E)$. This analysis also applies to $D^{K'\downarrow}(B,E)$ and $D^{K\downarrow}(B,E)$ but not to the case of $\Delta + \lambda_1 \neq -\Delta + \lambda_2$.

B. $\Delta_{\xi s_z} = 0$ and $\Delta \neq 0$

In this situation, the condition $\Delta_{\xi s_z} = 0$ will not be simultaneously satisfied for $K\uparrow$ and $K\downarrow$ if $\Delta \neq 0$. In other words, either the $K\uparrow$ electrons or the $K'\downarrow$ electrons have linear dispersion. For definiteness, we take $\Delta = 10$ meV, $\lambda_1 = -\Delta$ and $\lambda_2 = \Delta$. For valley $K(\xi = 1)$ and spin $\uparrow$ ($s_z = 1$) or valley $K'(\xi = -1)$ and spin $\downarrow$ ($s_z = -1$) in the graphene/TMD system, the Hamiltonian in Eq. (2) becomes the gapless one which is similar to the monolayer graphene. The energy bands for the $K\uparrow$ and $K'\downarrow$ electrons will turn into Dirac cones with linear dispersion as shown in Fig. 4(a). The energy spectra for the $K\uparrow$ and $K'\downarrow$ electrons will be similar to those in Fig. 3, which are not presented here.

For valley $K(\xi = 1)$ and spin $\downarrow$ ($s_z = -1$) or valley $K'(\xi = -1)$ and spin $\uparrow$ ($s_z = 1$) in the graphene/TMD system, the Hamiltonian in Eq. (2) is similar to the one for monolayer graphene with the staggered potential Δ. A gap 2Δ will open in the energy bands and the dispersion is of the parabolic form as shown in Fig. 4(a). The projection of the Berry curvatures in Eq. (5) will turn into a disk in the momentum space, which is centered at $k = 0$. When the field is raised from $B = -10T$, the closed path in the momentum space will enclose more area of the disk. The Berry phase will gradually increase as shown in Fig. 4(b). According to Eq. (18), the levels also alter gradually as given in Figs. 5(a) and 5(b) for $M = 0$ and $M = -1$, respectively.

We can understand the continuously changed levels more clearly in the following manner. If we keep $\lambda_1 = -\Delta$ and $\lambda_2 = \Delta$ but raise Δ from 0 to 10 meV, the Berry phase will evolve from the jump structure to the structure with the

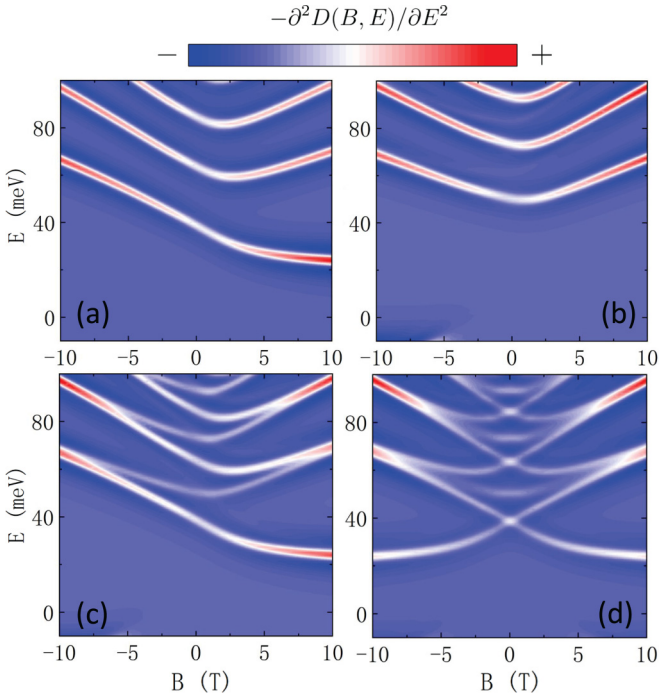

FIG. 5. The LDOS for valley K and spin $\downarrow$ electrons with (a) $M = 0$ and (b) $M = -1$. (c) The LDOS for $K\downarrow$ electrons contributed from $M = 0, \pm 1$. (d) The LDOS $D^{K\downarrow}(B,E) + D^{K'\uparrow}(B,E)$ contributed from $-10 \leqslant M \leqslant 10$. The parameters are taken as $\Delta = 10\,\text{meV}$, $\lambda_1 = -10\,\text{meV}$, $\lambda_2 = 10\,\text{meV}$, and $r = 0$.

gradual change. The levels evolve from the sudden jump to the continuous variation accordingly, which causes the connections of levels for $B < 0$ to lower (higher) levels for $B > 0$ in Fig. 3(a) [3(b)]. After the connections, the continuous energy spectra in Figs. 5(a) and 5(b) will be realized. If we plot the energy spectra for $M = 0$ and $M = \pm 1$ together, the obvious degeneracy-splitting-recombination behavior will be observed as given in Fig. 5(c). The LDOS $D^{K\downarrow}(B,E) + D^{K'\uparrow}(B,E)$ contributed from the different quantum numbers $M(-10 \leqslant M \leqslant 10)$ are also given in Fig. 5(d). The energy spectra in Fig. 5(d) are valley polarized. In other words, the energy spectra for $D^{K\downarrow}(B,E)$ and those for $D^{K'\uparrow}(B,E)$ can be well distinguished, which are symmetric about $B = 0$. Furthermore, the sudden jump and degeneracy-splitting-recombination behaviors can coexist in the graphene/TMD system if the $K\uparrow$ and $K'\downarrow$ electrons are also considered.

C. $\Delta_{\xi s_z} \neq 0$

We take $\Delta = 5\,\text{meV}$ and $\lambda_1 = \lambda_2 = -\Delta$. The energy bands for both $K\uparrow$ and $K\downarrow$ electrons open the same gap 2Δ as shown in Fig. 6(a). Their Berry phases change continuously when the field is increased from $-10T$ to $10T$, as presented in Fig. 6(b). The spin-valley dependent LDOS $D^{\xi s_z}(B,E)$ exhibit the degeneracy-splitting-recombination behaviors similar to those in Fig. 4(c). The LDOS $D^{\xi s_z}(B,E)$ are not degenerate. The LDOS $D^{\xi s_z}(B,E)$ and $D^{\bar{\xi}\bar{s}_z}(B,E)$ are symmetric about $B = 0$ since the time-reversal relation is satisfied by the two valleys. A relative translation of about 2Δ exists between the

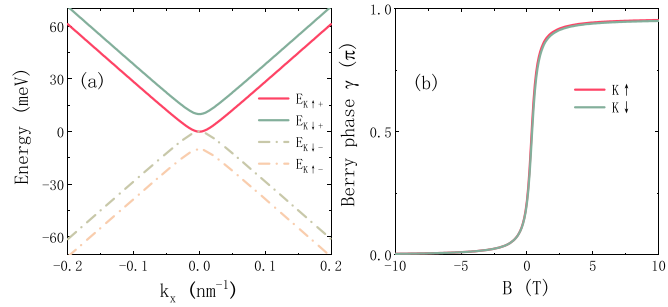

FIG. 6. (a) The energy bands for valley K under the parameters $\Delta = 5\,\text{meV}$, $\lambda_1 = -5\,\text{meV}$, and $\lambda_2 = -5\,\text{meV}$. The electrons with spin $\uparrow$ and spin $\downarrow$ both have parabolic dispersions. (b) The continuous change of Berry phase from 0 to π for the electrons with spin $\uparrow$ and spin $\downarrow$. Other parameters are taken as $M = 1$ and $E = 120\,\text{meV}$.

LDOS $D^{\xi s_z}(B,E)$ and $D^{\xi\bar{s}_z}(B,E)$ because of the spin polarization. These spin-valley-resolved features are still visible in the total LDOS $D(B,E)$ as the sum of the spin-valley dependent $D^{\xi s_z}(B,E)$ (see Fig. 7), which provide the possibility of designing the spin-valley polarized devices.

Recently, the perfect spin- and valley-polarized transport in the magnetic WSe_2 superlattice has been proposed [37]. There, the regulation of the dispersions (linear ones or parabolic ones) of electrons can be fulfilled by the nonresonance light. The switch and control of the polarized transport are implemented by the exchange field and gate voltages. Here, we shortly discuss the experimental realization of the spin-valley-polarized electron transport based on the circular quantum dot and the controllable Berry phase. The device may be designed as a two-terminal setup which consists of the nanoribbon of the graphene/TMD system attached by

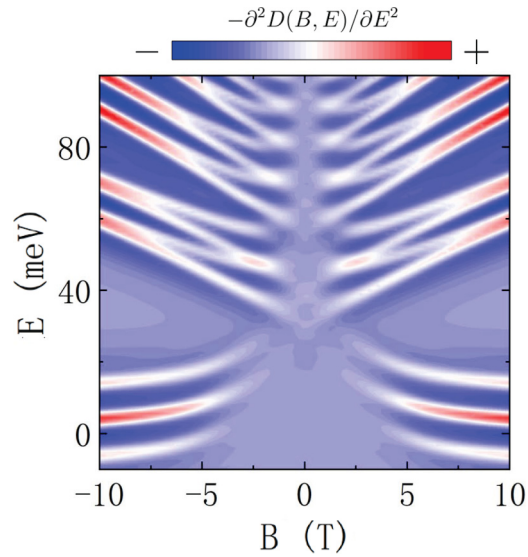

FIG. 7. The LDOS contributed from the two valleys and the two spins. The parameters are taken as $\Delta = 5\,\text{meV}$, $\lambda_1 = -5\,\text{meV}$, $\lambda_2 = -5\,\text{meV}$, and $r = 0$. The contributions from $-10 \leqslant M \leqslant 10$ have been considered.

the left and right electrodes [8]. The voltages are applied to the two electrodes and a circular quantum dot in the graphene/TMD system can be generated by the STM tip [10,32]. The Berry curvatures and the Berry phase of the electrons in the quantum dot can be tuned by a perpendicular field. When the nonpolarized current from one terminal flows through the quantum dot, it will be filtered into the spin-valley polarized one. Alternatively, the nanoribbon can be replaced by the graphene-based structure, which has been described by the similar Hamiltonian with the graphene/TMD system [38,39].

D. Evolutions of the energy spectra with the pseudospin potential and the spin-orbit coupling

In the above subsections, we have discussed in detail the evolutions of the energy spectra with the magnetic field for the different values of the pseudospin potential and the spin-orbit coupling. The evolutions exhibit the sudden jumps of the levels or the continues changes for the specific values of the potential and the coupling. In this subsection, we give the evolutions of the energy spectra with the potential and the coupling for the different fields taking the $K\uparrow$ electrons as an example. For $B=-1T$, the energy spectra vary continuously with the increase of the coupling λ_2 and the potential Δ as shown in Figs. 8(a) and 8(d). The Berry phase changes from $\gamma\approx 0$ to $\gamma\approx 2\pi$ when λ_2 is increased across $\lambda_2=10\,\text{meV}$ and from $\gamma\approx 2\pi$ to $\gamma\approx 0$ when Δ is increased across $\Delta=0$. The change of the Berry phase will cause the continuous variation of the level from the nth one to the $(n\pm 1)$th one according to Eq. (18) but will not cause the sudden jumps. However, for $B=0.2T$, the jumps of the levels at $\lambda_2=10\,\text{meV}$ or $\Delta=0$ happen as shown in Figs. 8(b) and 8(e). The Berry phase in this situation has an rapid change of about π when λ_2 is altered across $\lambda_2=10\,\text{meV}$ or Δ is altered across $\Delta=0$. It is noteworthy that the energy splitting ΔE is about half of the energy spacing. This is the representative effect realized in the quantum dot formed in the isolated graphene monolayer through tuning the magnetic field [7]. In the graphene/TMD system, the effect can also be realized by adjusting the pseudospin potential or the spin-orbit coupling for a given field, which is absent in the isolated graphene. If we continue to increase the magnetic field to $B=1T$, the variation of the Berry phase becomes the gradual change and the energy spectra become continuous accordingly, as shown in Figs. 8(c) and 8(f).

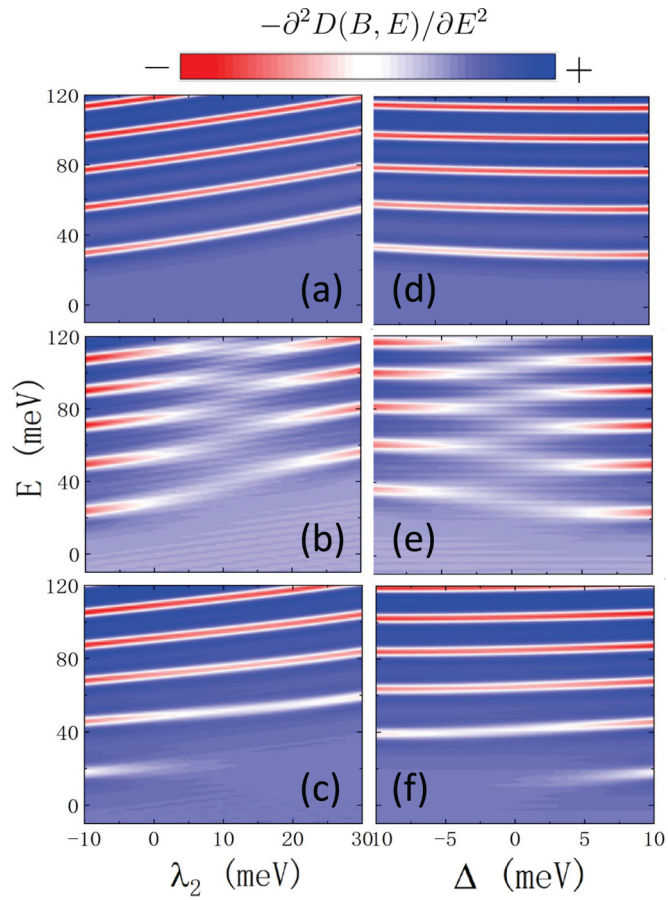

FIG. 8. The LDOS of the electrons from valley K with up spin in the (E,λ_2) space for $\Delta=10\,\text{meV}$ in (a)–(c) or in the (E,Δ) space for $\lambda_2=-10\,\text{meV}$ in (d)–(f). The value of the magnetic field is taken as $B=-1T$ in (a) and (d), $B=0.2T$ in (b) and (e), and $B=1T$ in (c) and (f). Other parameters are taken as $M=1$ and $\lambda_1=-10\,\text{meV}$.

IV. CONCLUSIONS

We study the features of the energy spectra in the quantum dot formed in the graphene/TMD system under a perpendicular field. The energy bands and the Berry curvatures for the electrons in the graphene/TMD system are analytically presented, which are strongly dependent on the pseudospin potential and the spin-orbit coupling parameters. For linear dispersion and point-shaped Berry curvatures, the Berry phase jumps when the field is altered while for the parabolic dispersion and the disk-shaped Berry curvatures, the Berry phase will continuously change. The energy spectra in the quantum dot of the graphene/TMD system can be tuned by the field through adjusting the Berry phase. They exhibit three typical features which are the pure sudden jumps of levels, the coexistence of the sudden jumps, and the degeneracy-splitting-recombination behaviors as well as the pure degeneracy-splitting-recombination behaviors. The evolutions of the energy spectra with the potential and the coupling from the sudden jumps to the continuous changes are investigated, which also originate from the rapid change and the gradual change of the Berry phase. These features of the energy spectra are peculiar to the graphene/TMD system and provide possible applications in spin-valleytronics.

ACKNOWLEDGMENTS

This work was financially supported by National Key R and D Program of China (Grant No. 2017YFA0303301), NSF-China under Grants No. 11921005 and No. 11447175, the Strategic Priority Research Program of Chinese Academy of Sciences (No. XDB28000000) and the Natural Science Foundation of Shandong Province under Grant No. ZR2017QA009.

[1] G. Giavaras and F. Nori, Phys. Rev. B **85**, 165446 (2012).
[2] P. Recher, J. Nilsson, G. Burkard, and B. Trauzettel, Phys. Rev. B **79**, 085407 (2009).
[3] D. R. da Costa, M. Zarenia, A. Chaves, G. A. Farias, and F. M. Peeters, Phys. Rev. B **92**, 115437 (2015).
[4] M. Mirzakhani, M. Zarenia, S. A. Ketabi, D. R. da Costa, and F. M. Peeters, Phys. Rev. B **93**, 165410 (2016).
[5] J. Lee, D. Wong, J. Velasco, Jr, J. F. Rodriguez-Nieva, S. Kahn, H.-Z. Tsai, T. Taniguchi, K. Watanabe, A. Zettl, F. Wang, L. S. Levitov, and M. F. Crommie, Nat. Phys. **12**, 1032 (2016).
[6] D. Xiao, M.-C. Chang, and Q. Niu, Rev. Mod. Phys. **82**, 1959 (2010).
[7] J. F. Rodriguez-Nieva and L. S. Levitov, Phys. Rev. B **94**, 235406 (2016).
[8] Z. Hou, Y.-F. Zhou, X. C. Xie, and Q.-F. Sun, Phys. Rev. B **99**, 125422 (2019).
[9] Y.-N. Ren, Q. Cheng, Q.-F. Sun, and L. He, arXiv:2108.07391.
[10] F. Ghahari, D. Walkup, C. Gutirrez, J. F. Rodriguez-Nieva, Y. Zhao, J. Wyrick, F. D. Natterer, W. G. Cullen, K. Watanabe, T. Taniguchi, L. S. Levitov, N. B. Zhitenev, and J. A. Stroscio, Science **356**, 845 (2017).
[11] Z. Y. Zhu, Y. C. Cheng, and U. Schwingenschlögl, Phys. Rev. B **84**, 153402 (2011).
[12] L. F. Mattheiss, Phys. Rev. B **8**, 3719 (1973).
[13] K. Kośmider, J. W. González, and J. Fernández-Rossier, Phys. Rev. B **88**, 245436 (2013).
[14] D. Xiao, G.-B. Liu, W. Feng, X. Xu, and W. Yao, Phys. Rev. Lett. **108**, 196802 (2012).
[15] W.-Y. Shan, H.-Z. Lu, and D. Xiao, Phys. Rev. B **88**, 125301 (2013).
[16] W. Feng, Y. Yao, W. Zhu, J. Zhou, W. Yao, and D. Xiao, Phys. Rev. B **86**, 165108 (2012).
[17] M. Tahir, P. M. Krstajić, and P. Vasilopoulos, Phys. Rev. B **95**, 235402 (2017).
[18] T. Cai, S. A. Yang, X. Li, F. Zhang, J. Shi, W. Yao, and Q. Niu, Phys. Rev. B **88**, 115140 (2013).
[19] N. D. Hien, C. V. Nguyen, N. N. Hieu, S. S. Kubakaddi, C. A. Duque, M. E. Mora-Ramos, L. Dinh, T. N. Bich, and H. V. Phuc, Phys. Rev. B **101**, 045424 (2020).
[20] V. Vargiamidis, P. Vasilopoulos, M. Tahir, and N. Neophytou, Phys. Rev. B **102**, 235426 (2020).
[21] A. Kormányos, V. Zólyomi, V. I. Fal'ko, and G. Burkard, Phys. Rev. B **98**, 035408 (2018).
[22] K.-H. Kim and H.-W. Lee, Phys. Rev. B **97**, 235423 (2018).
[23] M. Gmitra and J. Fabian, Phys. Rev. B **92**, 155403 (2015).
[24] M. Gmitra, D. Kochan, P. Högl, and J. Fabian, Phys. Rev. B **93**, 155104 (2016).
[25] T. Wakamura, F. Reale, P. Palczynski, S. Guéron, C. Mattevi, and H. Bouchiat, Phys. Rev. Lett. **120**, 106802 (2018).
[26] Z. Wang, D.-K. Ki, H. Chen, H. Berger, A. H. MacDonald, and A. F. Morpurgo, Nat. Commun. **6**, 8339 (2015).
[27] T. P. Cysne, J. H. Garcia, A. R. Rocha, and T. G. Rappoport, Phys. Rev. B **97**, 085413 (2018).
[28] M. Zubair, P. Vasilopoulos, and M. Tahir, Phys. Rev. B **101**, 165436 (2020).
[29] K. Zollner, A. W. Cummings, S. Roche, and J. Fabian, Phys. Rev. B **103**, 075129 (2021).
[30] C. Ke, Y. Wu, W. Yang, Z. Wu, C. Zhang, X. Li, and J. Kang, Phys. Rev. B **100**, 195435 (2019).
[31] S. Zihlmann, A. W. Cummings, J. H. Garcia, M. Kedves, K. Watanabe, T. Taniguchi, C. Schönenberger, and P. Makk, Phys. Rev. B **97**, 075434 (2018).
[32] Y.-N. Ren, Q. Cheng, S.-Y. Li, C. Yan, Y.-W. Liu, K. Lv, M.-H. Zhang, Q.-F. Sun, and L. He, Phys. Rev. B **104**, L161408 (2021).
[33] T. Habe and M. Koshino, Phys. Rev. B **96**, 085411 (2017).
[34] P. Högl, T. Frank, K. Zollner, D. Kochan, M. Gmitra, and J. Fabian, Phys. Rev. Lett. **124**, 136403 (2020).
[35] M. A. de Gosson, *Born-Jordan quantization: Theory and Applications* (Springer, Cham, Switzerland, 2016).
[36] C.-H. Park and N. Marzari, Phys. Rev. B **84**, 205440 (2011).
[37] Y. Hajati, M. Alipourzadeh, and I. Makhfudz, Phys. Rev. B **104**, 205402 (2021).
[38] D. Kochan, S. Irmer, and J. Fabian, Phys. Rev. B **95**, 165415 (2017).
[39] M. Gmitra, D. Kochan, and J. Fabian, Phys. Rev. Lett. **110**, 246602 (2013).